International Journal of Computer Information Systems and Industrial Management Applications
ISSN 2150-7988 Volume 18(3s) 2026 pp. 1397-1412
https://doi.org/10.70917/ijcisim-2026-2468
Article

Analytical Investigation of Laminar Dusty Fluid Flow and Thermal Non-Equilibrium Heat Transfer in an Asymmetric Corrugated Channel with Heat Source

Rohith Roshan A[1], Panneerselvi R[2], Dineshkumar S[3], Sumathi K[4*]

[1]Department of Mechanical Engineering, Engineering Design Division College of Engineering, Guindy, Chennai.600025.
rohithroshanarun@gmail.com
[3]Department of Mathematics, Dr. N.G.P. Institute of Technology, Coimbatore 641 048, Tamilnadu, India
Mail id: dineshsaravananmaths@gmail.com
[2,4]Department of Mathematics, PSGR Krishnammal College for Women, Coimbatore 641 004, Tamilnadu, India
panneerselvir09@gmail.com , ksumathi@psgrkcw.ac.in / sumathiarunmath@gmail.com

Abstract: This study presents an analytical investigation of the steady, two-dimensional laminar flow of an incompressible, viscous, dusty fluid contained within an asymmetric corrugated channel under thermal non-equilibrium conditions with internal heat generation. A stationary flat right wall and a stationary left wall with a sinusoidal corrugation define the channel geometry. The carrier fluid is embedded with a uniform distribution of rigid, small, spherical dust particles in the multi-phase system. A state of thermal non-equilibrium is explicitly considered to account for independent temperature variations between the phases. The governing nonlinear equations are non-dimensionalized and solved analytically using a regular perturbation technique for small wall corrugation amplitudes. The effects of the Reynolds number, Grashof number, Prandtl number and heat source parameter on the velocity and temperature distributions are investigated. The corresponding skin friction coefficients and local Nusselt numbers at both channel boundaries are also evaluated. The nonlinear influence and interaction of the governing parameters are further examined using Response Surface Methodology (RSM).

Keywords: Dusty fluid; Thermal non-equilibrium; Asymmetric corrugated channel; Heat generation; Perturbation analysis; Skin friction; Nusselt number.

1. Introduction

The transport of particulate-laden fluids through confined geometries has attracted considerable attention due to its importance in numerous engineering and industrial applications, including compact heat exchangers, microfluidic devices, filtration systems, petroleum transport, aerosol technology, and chemical processing. The presence of suspended solid particles significantly modifies the momentum and heat transfer characteristics of the carrier fluid, leading to complex two-phase interactions that cannot be adequately described by single-phase flow models. Saffman (1962) developed the fundamental mathematical formulations for two-phase particulate flows, treating the fluid phase as a continuum of uniform, rigid spheres that only interact with a carrier fluid through linear Stokes drag. This led to the scientific development of two-phase fluid flows. Following this breakthrough, early researchers focused heavily on mapping exact analytical solutions for highly idealized geometries. By solving steady and transient flows between infinite flat plates, Michael (1965) and Healy and Yang (1970) demonstrated that the presence of dust particles introduces a relaxation time that effectively dampens fluid velocity transitions, advancing our understanding of fundamental dusty fluid configurations.

Datta and Mishra (1982) showed that the fluid-particle interaction parameter alters the classical Stokes boundary layer thickness and extended these classical configurations to oscillating systems. Due to its relevance to

surface roughness and heat transfer enhancement, the investigation of fluid flows over wavy or corrugated surfaces emerged as a distinct area of interest concurrently. Benjamin's seminal analysis of shearing flows over wavy boundaries in 1959 showed how shifting pressure distributions are caused by periodic wall fluctuations. Vajravelu and Sastry (1978) focused specifically on the free convective heat transfer of a viscous fluid enclosed between a vertical flat wall and a long wavy wall.

Burns and Dutcher (2010), who quantified how the aspect ratios and periodic walls of channels can be manipulated to alter laminar flow features, maximize lateral mixing, and affect pressure drop parameters, later applied this geometric problem to microfluidics. Borkakati and Pop (1984) were the first to investigate the convergence of these two distinct pathways—dusty fluids and corrugated boundaries—by evaluating the unsteady hydromagnetic flow of a dusty viscous fluid bounded by a parallel flat wall and a long wavy wall. Ghosh and Debnath (2004) expanded on this phenomenon by providing precise solutions for dusty fluid tracking between a non-torsionally oscillating plate and a wavy boundary. Turkyilmazoglu (2012) conducted a comprehensive analytical verification of boundary layer flows in dusty fluids, demonstrating that when a fluid-particle mixture undergoes rapid acceleration over a surface, the thermal fields decouple from the velocity fields, necessitating an independent energy equation for the particulate phase. Ramesh *et al.* (2012) looked at the thermal characteristics of dusty fluid flows over stretching sheets to describe these decoupled fields. Similarly, Gireesha *et al*. (2012) utilized numerical schemes to analyse the heat transfer in dusty fluids under the influence of non-uniform heat sources, establishing that thermal non-equilibrium significantly alters the Nusselt number along solid boundaries.

In recent studies, complex fluid rheology and porous media have been heavily incorporated into these geometric configurations to simulate industrial filters and fractures. Umavathi *et al.* (2005) carried out a comprehensive investigation into the convective flow of a fluid within a wavy channel that was filled with porous media. Multi-component fluids moving over permeable surfaces were successfully analyzed using multi-phase approximations by Mahanthesh *et al*. (2017), confirming that particulate drag and viscous dissipation can reduce fluid velocity while stabilizing the thermal boundary layer. Additionally, non-Newtonian frameworks have been introduced to dusty fluid domains; Siddiqa *et al*. (2015) simulated the flow of a dusty non-Newtonian fluid over stretching surfaces, proving that increasing fluid-particle interactions enhance skin friction while causing substantial changes in the clean fluid's convective heat transfer profile.

The particular issue of a fluid bounded symmetrically or asymmetrically by a sinusoidally corrugated wall and a flat wall continues to be the focus of optimization research. Early numerical mapping of heat transfer in corrugated channels by Asako and Faghri (1987) laid the groundwork for the modern compact heat exchanger designs described by Nishimura *et al.* (1984). These investigators proved that wall-curvature-induced swirl is highly dependent on the wavelength and amplitude ratios of the corrugations. According to a recent study by Chamkha (2000), when particles are added to these configurations, the rigid spheres' spatial distribution becomes non-uniform due to centrifugal forces in the wall troughs.

Attia (2006) established how magnetic parameters impact the velocity profiles of dusty fluids during transient behaviour, while Hayat *et al*. (2012) examined the influence of radiative heat transfer on multi-phase flows, noting that thermal radiation speeds up the decoupling of thermal fields under non-equilibrium conditions. Entropy generation analysis was used by Rashidi *et al*. (2014) to optimize these parameters, confirming that geometric channels reduce thermal losses. Unsteady laminar flow (Nield & Kuznetsov, 2009), dusty fluids (Saffman, 1962), corrugated channels (Wang & Chen, 2002), and thermal non-equilibrium (Turkyilmazoglu, 2012) are just a few of the physical system's components that have received individual attention, but their combined and simultaneous interaction is still a mystery.

A unified model for how an asymmetric, sinusoidally corrugated channel boundary interacts with the unsteady momentum of a dusty phase while maintaining a decoupled thermal field is currently lacking in the literature. This paper addresses this specific research gap.

2. Mathematical formulation

Consider a steady, two-dimensional, laminar flow of an incompressible viscous dusty fluid confined between a stationary flat right wall and a stationary sinusoidally corrugated left wall. The carrier fluid contains uniformly distributed rigid spherical dust particles. The two phases interact through Stokes drag, while thermal equilibrium between the fluid and dust phases is not assumed. The channel boundaries are $y^* = d^*$ and $y^* = \epsilon^* cos\left(\frac{2\pi}{\gamma}x^*\right)$. The flow is assumed to occur in the positive x-direction under the combined influence of an imposed pressure

gradient and buoyancy forces. Thermal non-equilibrium is assumed between the fluid and particle phases, allowing each phase to possess its own temperature field.

Assumptions:

- The flow is steady, laminar, and two-dimensional.
- The carrier fluid is Newtonian, viscous, and incompressible.
- Dust particles are rigid, spherical, and uniformly distributed.
- The particle volume fraction is sufficiently small so that particle-particle interactions are neglected.
- The interaction between the fluid and particle phases occurs only through linear Stokes drag.
- Fluid properties are constant except for the density variation in the buoyancy term, where the Boussinesq approximation is invoked.
- Viscous dissipation and thermal radiation are neglected.
- The wall corrugation amplitude is small ($\varepsilon \ll 1$), permitting the application of the regular perturbation method.
- Thermal relaxation time is <<1.
- Particle loading is low. Therefore , N is assumed constant.

Based on these assumptions, the governing equations for an incompressible viscous fluid are

For fluid phase

$$\nabla \cdot \vec{q}^* = 0 \tag{1}$$

$$\rho_0[(\vec{q}^*, \nabla^*)\vec{q}^*] = -\nabla^* p^* - \rho_0 g \beta_T (T - T_0)\hat{\imath} + \mu \nabla^{*2} \vec{q}^* + KN\left(\vec{q}_p^* - \vec{q}^*\right) \tag{2}$$

$$\rho c_p (\vec{q}^* \cdot \nabla^*) T^* = \kappa \nabla^{*2} T^* - Q^*(T - T_0) \tag{3}$$

For particle phase

$$\nabla^* \cdot \vec{q}_p^* = 0 \tag{4}$$

$$m_p N\left(\vec{q}_p^* \cdot \nabla^*\right)\vec{q}_p^* = KN\left(\vec{q}^* - \vec{q}_p^*\right) \tag{5}$$

The corresponding boundary conditions

$$u^* = 0; \quad v^* = 0; \quad u_p{}^* = 0; \quad v_p{}^* = 0; T^* = T_0 \text{ at } \quad y^* = \epsilon^* cos\left(\frac{2\pi}{\gamma} x^*\right)$$

$$u^* = 0; \quad v^* = 0; \quad u_p{}^* = 0; \quad v_p{}^* = 0; T^* = T_1 \text{ at } \quad y^* = d^* \tag{6}$$

By introducing the following dimensionless parameters,

$$(x^*, y^*, z^*) = d^*(x, y, z); p^* = \rho_0 U_0^2 p; (u^*, v^*, w^*) = \mathrm{U}_0(u, v, w)$$

$$(u_d^*, v_d^*, w_d^*) = \mathrm{U}_0(u_d, v_d, w_d); \ \frac{\mathrm{T} - T_0}{T_1 - T_0} = \theta; \tag{7}$$

Here, p is the non-dimensional pressure, ρ is the density of the fluid, N is the number density of the dust particle, K is the stokes drag constant, m_p is the mass of the dust particle, respectively.

Hence the non-dimensional equations are

For Fluid phase

$$\nabla \cdot \vec{q} = 0 \tag{8}$$

$$(\vec{q} \cdot \nabla)\vec{q} = -\nabla \rho \ - \frac{Gr}{Re^2}\theta\hat{\imath} + \frac{1}{R_e}\nabla^2 \vec{q} + \beta\left(\vec{q}_p - \vec{q}\right) \tag{9}$$

$$(\vec{q} \cdot \nabla)\theta = \frac{1}{\mathrm{Pr.Re}}\nabla^2 \theta - Q\theta \tag{10}$$

For Particle phase

$$\nabla \cdot \vec{q}_p = 0 \tag{11}$$

$$(\vec{q}_p \cdot \nabla)\vec{q}_p = \frac{\beta}{L}(\vec{q} - \vec{q}_p) \quad (12)$$

where, $\Pr = \frac{\mu C_P}{K}$ (Prandtl number), $Re = \frac{U_0 d^*}{\nu}$(Reynolds number), $\beta = \frac{KNd}{\rho U_0}$ (Drag parameter)

$L = \frac{\rho_d}{\rho}$ (Particle loading parameter), $Q = \frac{Q^* d}{\rho C_p U_0}$ (Heat absorption/generation parameter)

$Gr = \frac{\rho g \beta_T (T - T_0)}{{U_0}^2}$(Grashof number for heat transfer)

The governing equations in component form are

For Fluid phase

$$\frac{\partial u}{\partial x} + \frac{\partial v}{\partial y} = 0 \quad (13)$$

$$u\frac{\partial u}{\partial x} + v\frac{\partial u}{\partial y} = -\frac{\partial p}{\partial x} + \frac{1}{R_e}\left[\frac{\partial^2 u}{\partial x^2} + \frac{\partial^2 u}{\partial y^2}\right] + \beta(u_p - u) + \frac{Gr}{Re^2}\theta \quad (14)$$

$$u\frac{\partial v}{\partial x} + v\frac{\partial v}{\partial y} = -\frac{\partial p}{\partial y} + \frac{1}{R_e}\left[\frac{\partial^2 v}{\partial x^2} + \frac{\partial^2 v}{\partial y^2}\right] + \beta(v_p - v) \quad (15)$$

$$u\frac{\partial \theta}{\partial x} + v\frac{\partial \theta}{\partial y} = \frac{1}{\Pr.\mathrm{Re}}\left(\frac{\partial^2 \theta}{\partial x^2} + \frac{\partial^2 \theta}{\partial y^2}\right) - Q\theta \quad (16)$$

For Particle phase

$$\frac{\partial u_p}{\partial x} + \frac{\partial v_p}{\partial y} = 0 \quad (17)$$

$$\left(u_p\frac{\partial u_p}{\partial x} + v_p\frac{\partial u_p}{\partial y}\right) = \frac{\beta}{L}(u - u_p) \quad (18)$$

$$\left(u_p\frac{\partial v_p}{\partial x} + v_p\frac{\partial v_p}{\partial z}\right) = \frac{\beta}{L}(v - v_p) \quad (19)$$

Subject to the boundary conditions

$$u = 0;\quad \mathrm{v} = 0;\quad u_p = 0;\quad v_p = 0;\ \theta = 0 \text{ at } \quad y = \epsilon cos\,(\alpha x)$$

$$u = 0;\quad v = 0;\quad u_p = 0;\quad v_p = 0;\ \theta = 1 \text{ at } \quad y = 1 \quad (20)$$

where ϵ - wave amplitude and α – wave number

3. Solution of the problem

In order to solve the differential equation (13) - (29), we assume the solution in the following form

$$u(x,y) = u_0(y) + \epsilon u_1(x,y) + \epsilon^2 u_2(x,y) + \cdots$$
$$v(x,y) = v_0(y) + \epsilon v_1(x,y) + \epsilon^2 v_2(x,y) + \cdots$$
$$\theta(x,y) = \theta_0(y) + \epsilon\theta_1(x,y) + \epsilon^2\theta_2(x,y) + \cdots$$
$$u_p(x,y) = u_{p_0}(y) + \epsilon u_{p1}(x,y) + \epsilon^2 u_{p2}(x,y) + \cdots$$
$$v_p(x,y) = v_{p_0}(y) + \epsilon v_{p_1}(x,y) + \epsilon^2 v_{p_2}(x,y) + \cdots$$
$$p(x,y) = p_0(y) + \epsilon p_1(x,y) + \epsilon^2 p_2(x,y) + \quad (21)$$

The wave amplitude ϵ is assumed to be small. When $\epsilon = 0$, the problem reduces to

$$\frac{\partial v_0}{\partial y} = 0\,, v_0 = 1 \quad (28)$$

$$\frac{1}{Re}\frac{\partial^2 u_0}{\partial y^2}+\frac{Gr}{Re^2}\theta_0=0 \quad (29)$$

$$-\frac{\partial P_0}{\partial y}=0 \Rightarrow\ p_0=k=1 \quad (30)$$

$$\frac{1}{PrRe}\frac{\partial^2 \theta_0}{\partial y^2}-Q\theta_0(y)=0 \quad (31)$$

$$\frac{\partial v_{p_0}}{\partial y}=0; v_{P_0}=1 \quad (32)$$

$$u_{p_0}=u_0 \quad (33)$$

With corresponding boundary conditions

$u_0=0; v_0=0;\ \ \theta_0=0, u_{p_0}=0;\ v_{p_0}=0$ at y = 0

$u_0=0; v_0=0;\ \ \theta_0=1, u_{p_0}=0;\ v_{p_0}=0$ at y = 1 (34)

Hence the solution is given by

$$u_0(y)=A_4 y-\frac{Gr}{Re}\left(\frac{A_1}{{m_1}^2}\right)(e^{m_1 y}-e^{m_2 y}) \quad (35)$$

$$u_{p_0}(y)_{=}u_0(y) \quad (36)$$

$$\theta_0(y)=A_1 e^{m_1 y}+A_2 e^{m_2 y} \quad (37)$$

$$v_o(y)=v_{p_0(y)}=p_0(y)=0 \quad (38)$$

When comparing the coefficients of ϵ and neglecting the higher order terms, we get the following equations

$$\frac{\partial u_1}{\partial x}+\frac{\partial v_1}{\partial y}=0 \quad (39)$$

$$\frac{\partial u_{p_1}}{\partial x}+\frac{\partial v_{p_1}}{\partial y}=0 \quad (40)$$

$$u_0\frac{\partial u_1}{\partial y}+v_1\frac{\partial u_0}{\partial y}=-\frac{\partial p_1}{\partial x}+\frac{1}{\mathrm{Re}}\left(\frac{\partial^2 u_1}{\partial x^2}+\frac{\partial^2 u_1}{\partial y^2}\right)+\beta\left(u_{p_1}-u_1\right)+\frac{Gr}{Re^2}\theta_0 \quad (41)$$

$$u_0\frac{\partial v_1}{\partial y}=-\frac{\partial p_1}{\partial y}+\frac{1}{\mathrm{Re}}\left(\frac{\partial^2 v_1}{\partial x^2}+\frac{\partial^2 v_1}{\partial z^2}\right)+\beta\left(v_{p_1}-v_1\right) \quad (42)$$

$$u_0\frac{\partial \theta_1}{\partial y}+v_1\frac{\partial \theta_0}{\partial y}=\frac{1}{\mathrm{Pr.Re}}\left(\frac{\partial^2 \theta_1}{\partial x^2}+\frac{\partial^2 \theta_1}{\partial y^2}\right)-\ Q\theta_1 \quad (43)$$

$$u_{\mathrm{p}_0}\frac{\partial u_{\mathrm{p}_1}}{\partial y}+v_{\mathrm{p}_1}\frac{\partial u_{\mathrm{p}_0}}{\partial y}=\frac{\beta}{L}\left(u_1-u_{p_1}\right) \quad (44)$$

$$u_{\mathrm{p}_0}\frac{\partial v_{\mathrm{p}_1}}{\partial y}=\frac{\beta}{L}\left(v_1-v_{p_1}\right) \quad (45)$$

To solve the equations (39) to (45) we assume the following form

$f_1(x,y)=e^{i\alpha x}\cdot f_{11}(y)$ we get

$$i\alpha u_{11}+\frac{\partial v_{11}}{\partial y}=0 \quad (46)$$

$$i\alpha u_{p_{11}}+\frac{\partial v_{p_{11}}}{\partial y}=0 \quad (47)$$

$$u_0 i\alpha u_{11}+v_{11}\frac{\partial u_0}{\partial y}=-i\alpha p_{11}+\frac{1}{\mathrm{Re}}\left(-\alpha^2+\frac{\partial^2}{\partial y^2}\right)u_{11}+\beta\left(u_{p_{11}}-u_{11}\right)+\frac{Gr}{Re^2}\theta_{11} \quad (48)$$

$$u_0 i\alpha v_{11}=-\frac{\partial p_{11}}{\partial y}+\frac{1}{\mathrm{Re}}\left(-\alpha^2+\frac{\partial^2}{\partial y^2}\right)v_{11}+\beta\left(v_{p_{11}}-v_{11}\right) \quad (49)$$

$$u_0 i\alpha\theta_{11}+v_{11}\frac{\partial \theta_0}{\partial y}=\frac{1}{\mathrm{Pr.Re}}\left(-\alpha^2+\frac{\partial^2}{\partial y^2}\right)\theta_{11}-\mathrm{Q}\theta_{11} \quad (50)$$

$$u_{p_0} i\alpha u_{p_{11}} + v_{p_{11}} \frac{\partial u_{p_0}}{\partial y} = \frac{\beta}{L}\left(u_{11} - u_{p_{11}}\right) \quad (51)$$

$$u_{p_0} i\alpha v_{p_{11}} = \frac{\beta}{L}\left(v_{11} - v_{p_{11}}\right) \quad (52)$$

The corresponding boundary conditions are

$$u_{11} = -u_0'(0);\ v_{11} = 0;\ \ \theta_{11} = -\theta_0'(0),\ u_{p_{11}} = -u_{p_0}'(0);\ \ v_{p_{11}} = 0 \quad \text{at y = 0}$$

$$u_{11} = 0;\ v_{11} = 0;\ \ \theta_{11} = 1,\ u_{p_{11}} = 0;\ \ v_{p_{11}} = 0 \quad \text{at y = 1} \quad (53)$$

Again assume $f_{11} = f_{110} + \alpha f_{111} + \ldots$ (54)

Substituting equation (54) in equations (46) – (53) and collecting the like powers of a, we get

$$u_{110} + \frac{\partial v_{111}}{\partial y} = 0 \quad (55)$$

$$u_{p_{110}} + \frac{\partial v_{p_{111}}}{\partial y} = 0 \quad (56)$$

$$\frac{1}{\mathrm{Re}} \frac{\partial^2 u_{110}}{\partial y^2} + \frac{Gr}{Re^2}\theta_{110} = 0 \quad (57)$$

$$u_0 i\alpha v_{11} = -\frac{\partial p_{11}}{\partial y} + \frac{1}{\mathrm{Re}}\left(-\alpha^2 + \frac{\partial^2}{\partial y^2}\right) v_{11} + \beta\left(v_{p_{11}} - v_{11}\right) \quad (58)$$

$$\frac{\partial p_{110}}{\partial y} = 0 \implies p_{110} = 1 \quad (59)$$

$$\frac{1}{\mathrm{Pr.Re}}\theta_{110} - \mathrm{Q}\theta_{110} = 0 \quad (60)$$

$$u_{110} - u_{p_{110}} = 0 \quad (61)$$

$$v_{111} - v_{p_{111}} = 0 \quad (62)$$

With corresponding boundary conditions

$$u_{110} = -u_0'(0);\ \ \theta_{110} = -\theta_0'(0) \ \text{ at y = 0}$$

$$u_{110} = 0 :\ \theta_{110} = 0 \quad \text{at y = 1} \quad (63)$$

$O(\alpha)$

$$\frac{\partial^2 v_{111}}{\partial z^2} = -i\mathrm{u}_{110} \quad (64)$$

By solving, we get

$$u_{110} = A_7 + A_8 y - \frac{Gr}{Re}\left(\frac{A_5}{{m_1}^2} e^{m_1 y} + \frac{A_6}{{m_2}^2} e^{m_2 y}\right) \quad (65)$$

$$\theta_{110} = A_5 e^{m_1 y} + A_6 e^{m_2 y} \quad (66)$$

$$v_{111} = -i\left(A_7 y + A_8 \frac{y^2}{2} - \frac{Gr}{Re}\frac{A_5}{{m_1}^3} e^{m_1 y} - \frac{Gr}{Re}\frac{A_5}{{m_2}^3} e^{m_2 y}\right) \quad (67)$$

4. Skin friction

The skin friction is given by

$$S_{k_{y = \epsilon cos(\alpha x)}} = \frac{1}{Re}\left(u_0'(0) + \epsilon cos\lambda x\left(u_0''(0) + u_1'(0)\right)\right) \quad (68)$$

$$S_{k_{y=1}} = \frac{1}{Re}\left(u_0'(1) + u_1'(1)\epsilon cos\lambda x\right) \quad (69)$$

5. Rate of heat transfer

The rate of heat transfer is given by

$$Nu_{y=\epsilon cos(\alpha x)} = -\theta_0'(0) + \epsilon cos\lambda x\left(\theta_0''(0) + \theta_{11}'(0)\right) \quad (70)$$

$$Nu_{y=1} = \theta_0'(1) + \theta_{11}'(1)\epsilon cos\lambda x \quad (71)$$

For the sake of brevity, the constants are given in *Appendix*.

6. Result and Discussion

Steady, two-dimensional, laminar flow of an incompressible viscous dusty fluid confined between a stationary flat right wall and a stationary sinusoidally corrugated left wall with heat source effect is considered for study. The results for various dimensionless parameters are discussed with the help of graphs.

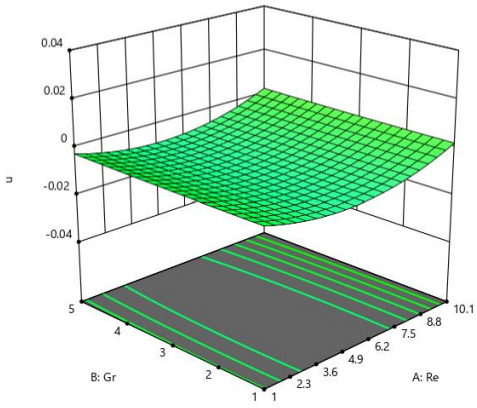

Fig. 1 Velocity profile for various Gr

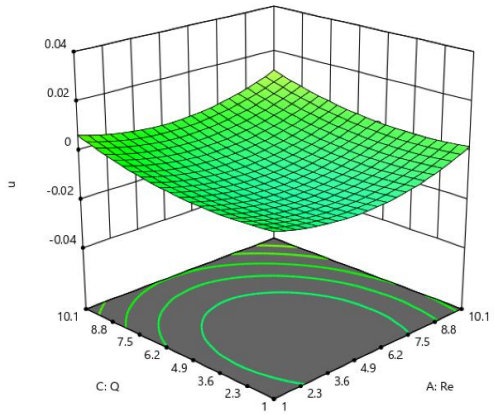

Fig. 2 Velocity profile for various Re

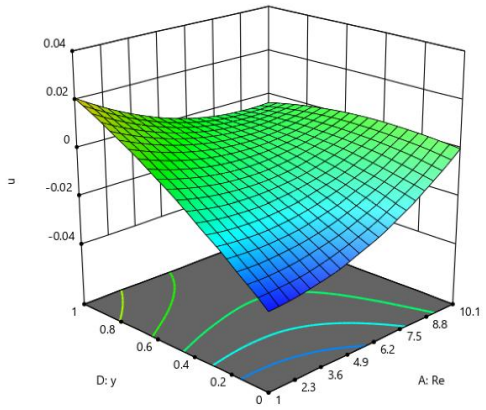

Fig. 3 Velocity profile for various Re

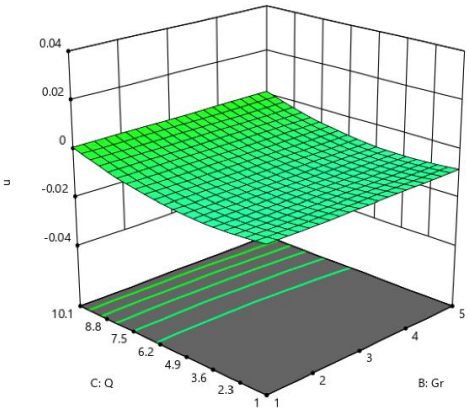

Fig. 4 Velocity profile for various Q

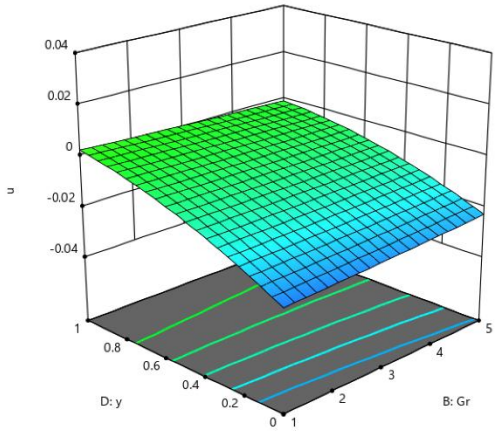

Fig. 5 Velocity profile for various Gr

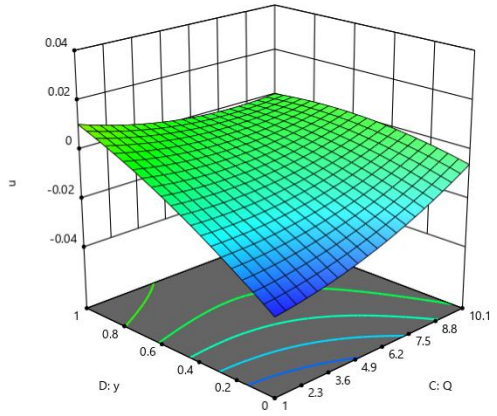

Fig. 6 Velocity profile for various Q

The quadratic response surface plots presented in figures 1-6 reveal the behaviour of the velocity as a function of the nondimensional parameters Gr, Pr, Re, Q. These illustrations show that the response variable exhibits nonlinear behaviour with respect to the investigated parameters. Among the variables, the transverse coordinate (**y**) exerts the strongest influence on the velocity response, followed by the Reynolds number (Re). The heat source parameter (Q) produces a moderate effect, whereas the Grashof number (Gr) has the least influence within the selected design space. Significant interaction effects are observed primarily between Re and Q and between Re and y, as evidenced by the curved response surfaces and elliptical contour patterns. In contrast, the interactions involving Gr are comparatively weak, with nearly parallel contour lines indicating minimal dependence between the variables. The smooth curvatures of the response surfaces confirm the suitability of the quadratic RSM model for representing the nonlinear relationships among the governing parameters.

The response surface plots represented in figures 7-12 clearly show the effect of Reynolds number (Re), Grashof number (Gr), Heat source parameter (Q), and transverse coordinate (y) on the temperature profile θ (theta). Since a quadratic RSM model has been used, the observed curvature indicates second-order effects of the input variables.

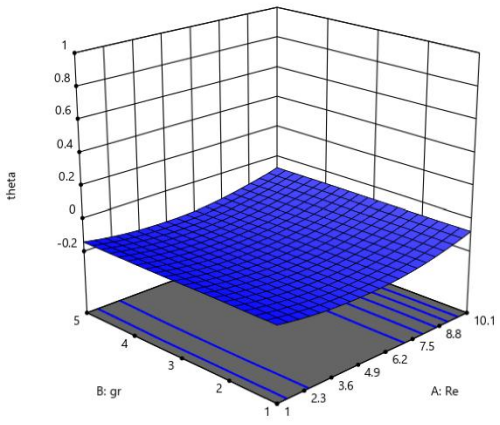

Fig. 7 Temperature profile for various Gr

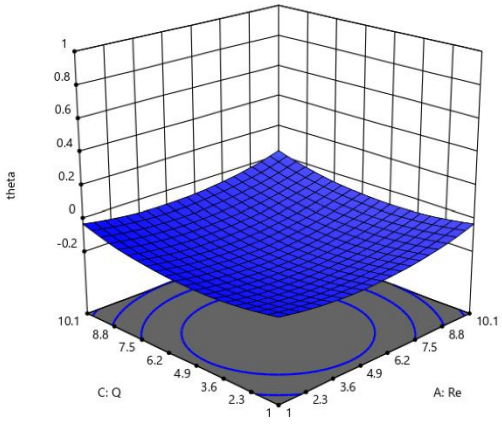

Fig. 8 Temperature profile for various Q

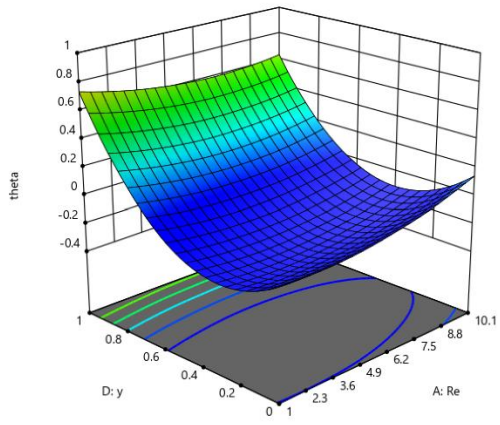

Fig. 9 Temperature profile for various Re

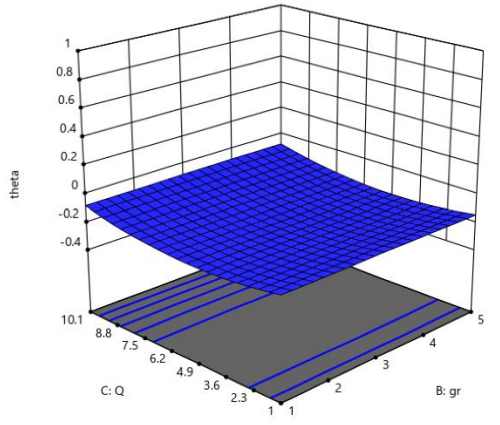

Fig. 10 Temperature profile for various Gr

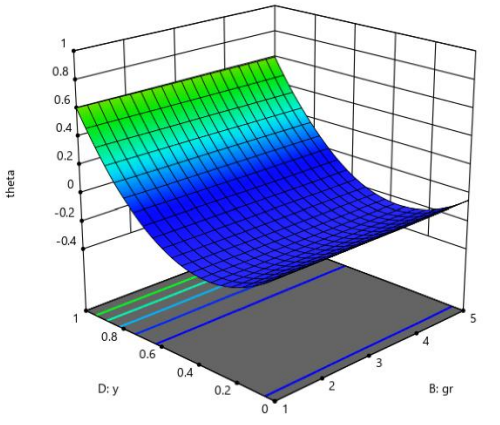

Fig. 11 Temperature profile for various Gr

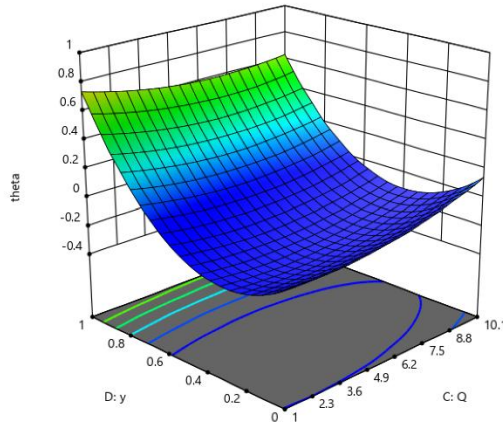

Fig. 12 Temperature profile for various Q

The response surface analysis demonstrates that the temperature profile exhibits a nonlinear dependence on the governing parameters, validating the applicability of the quadratic response surface model. Among the investigated variables, the transverse coordinate **(y)** has the most significant influence on the temperature distribution, producing a substantial increase in the response throughout the domain. Reynolds number exhibits a moderate inverse effect owing to enhanced convective heat transport, whereas the influences of the Grashof number and the heat source parameter are comparatively smaller within the selected parameter range. Noticeable interaction effects are observed primarily for the Re-Q and Re-y combinations, as indicated by the curved response surfaces and elliptical contour patterns. In contrast, interactions involving the Grashof number are relatively weak, evidenced by the nearly parallel contour lines. The smooth quadratic surfaces and absence of abrupt changes indicate stable nonlinear behaviour and confirm the adequacy of the fitted quadratic RSM model for predicting the temperature response.

The RSM plots given in figures 13-18 correspond to the response Nusselt number at the wavy plate (Nu) as a function of Re, Gr, Q, and Pr. The response surfaces exhibit smooth quadratic curvature, confirming that the quadratic RSM model adequately represents the nonlinear heat transfer characteristics.

The quadratic response surface analysis reveals that the Nusselt number at the wavy plate is governed by nonlinear relationships among the governing parameters. Reynolds number and Prandtl number exert the strongest influence on heat transfer. Reynolds number exhibits an optimum value, beyond which the Nusselt number decreases, confirming the existence of a significant quadratic effect. In contrast, increasing the Prandtl number consistently enhances the Nusselt number owing to improved thermal diffusion characteristics and reduced thermal boundary layer thickness. The Grashof number and heat source parameter have comparatively smaller effects on the

response within the investigated parameter range. Significant interaction effects are observed primarily for the Re-Pr and Re-Gr combinations, while interactions involving Q are relatively weak. The smooth response surfaces and elliptical contour patterns confirm the adequacy of the quadratic RSM model for accurately predicting the Nusselt number over the experimental domain.

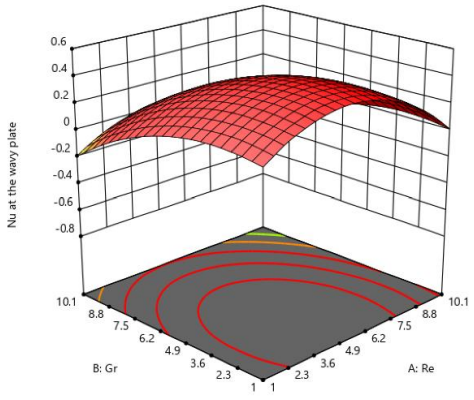

Fig. 13 Nu at wavy plate for various Gr

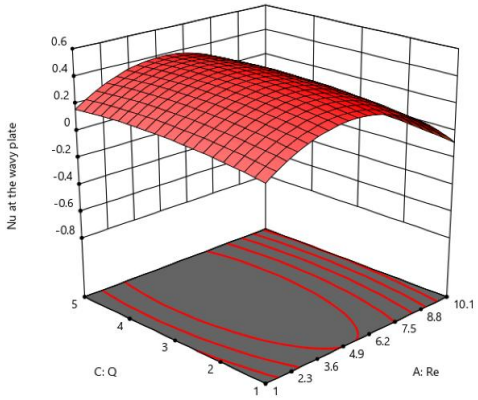

Fig. 14 Nu at wavy plate for various Re

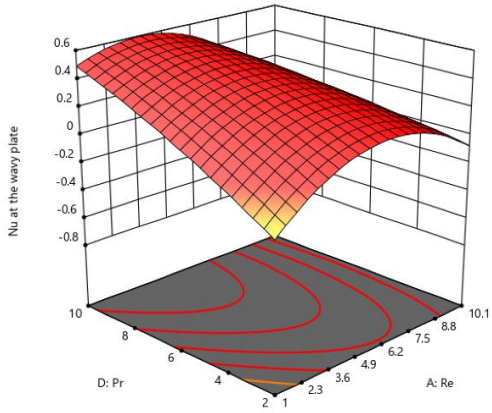

Fig. 15 Nu at wavy plate for various Pr

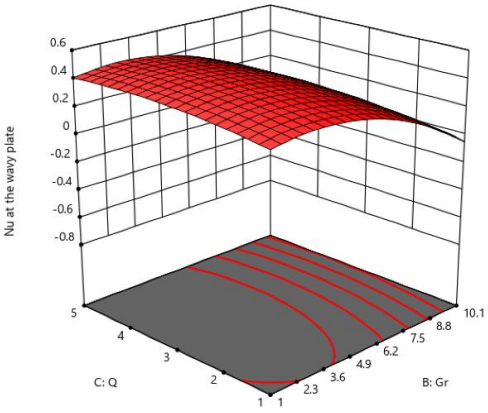

Fig. 16 Nu at wavy plate for various Q

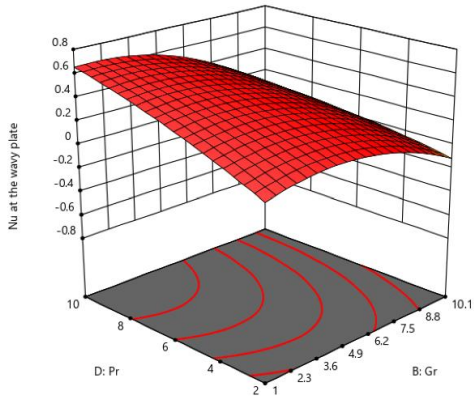

Fig. 17 Nu at wavy plate for various Gr

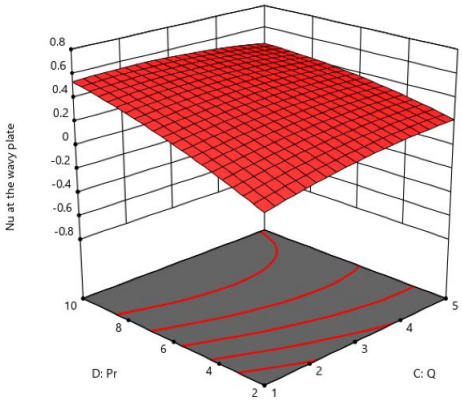

Fig. 18 Nu at wavy plate for various Q

The response surface plots illustrated in Figures 19-24 represent the effect of Reynolds number (Re), Grashof number (Gr), Heat source parameter (Q), and Prandtl number (Pr) on the Nusselt number at the wall y=1. The

smooth nonlinear surfaces confirm the adequacy of the quadratic RSM model in describing the heat transfer characteristics.

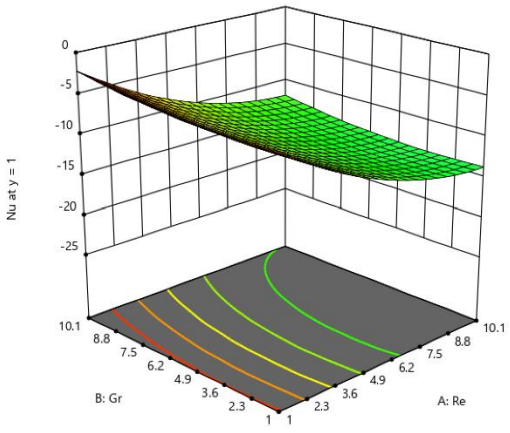

Fig. 19 Nu at y =1 for various Gr

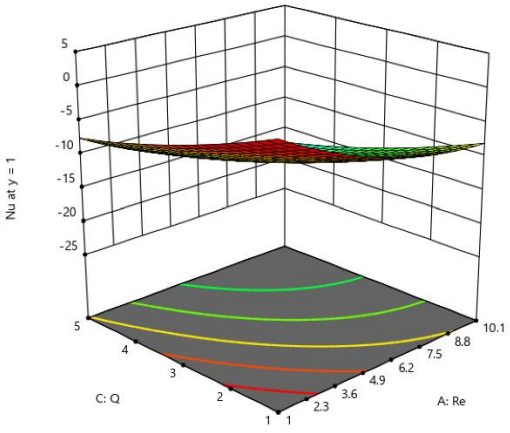

Fig. 20 Nu at y =1 for various Gr

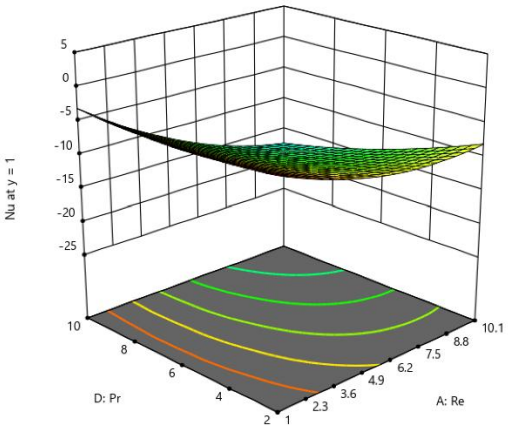

Fig. 21 Nu at y =1 for various Pr

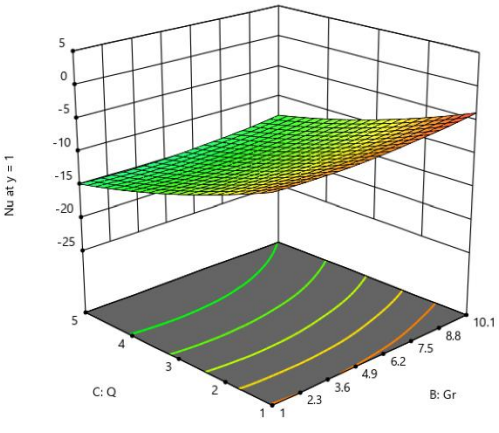

Fig. 22 Nu at y =1 for various Q

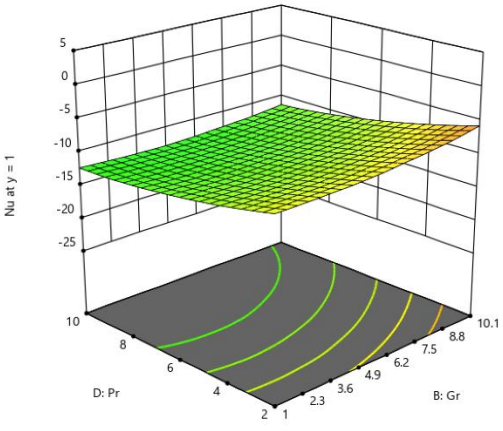

Fig. 23 Nu at y =1 for various Gr

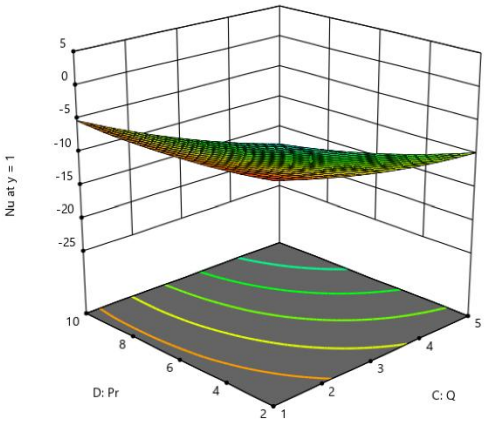

Fig. 24 Nu at y =1 for various Pr

The response surface analysis indicates that the local Nusselt number at the wall y=1 exhibits nonlinear dependence on the governing parameters, confirming the suitability of the quadratic RSM model. Among the

investigated variables, Reynolds number has the strongest negative influence on the wall Nusselt number, whereas the Prandtl number has the most significant positive influence owing to the reduction in thermal boundary layer thickness. The Grashof number provides a mild enhancement in heat transfer through buoyancy effects, while the heat source parameter exerts only a moderate influence. Interaction effects among the variables are generally weak to moderate, as indicated by the gently curved response surfaces and contour plots. No sharp peaks or abrupt transitions are observed, suggesting stable nonlinear behaviour throughout the design space and demonstrating that the fitted quadratic model adequately predicts the local heat transfer characteristics.

These response surface plots shown in Figures 25-27 depict the influence of Grashof number (Gr), Heat source parameter (Q), and Prandtl number (Pr) on the skin friction coefficient (Sk) at the wavy wall. The fitted quadratic model predicts a smooth nonlinear variation of the skin friction coefficient over the design space.

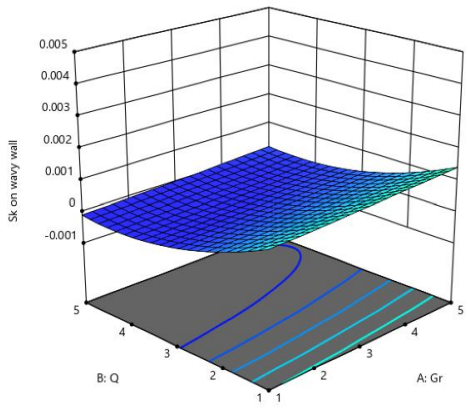

Fig. 25 Skin friction at wavy wall for various Gr

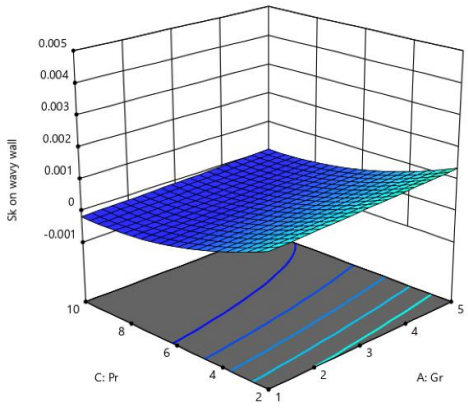

Fig. 26 Skin friction at wavy wall for various Pr

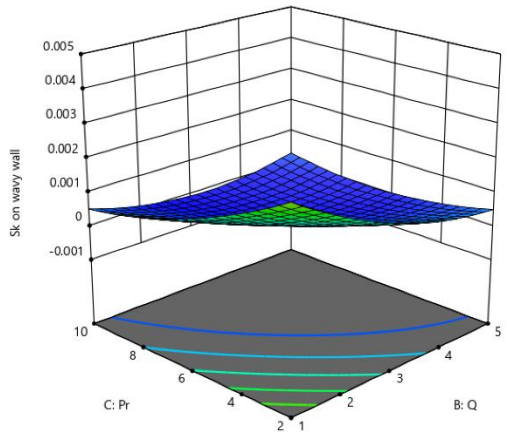

Fig. 27 Skin friction at wawvy wall for various Q

The quadratic response surface analysis indicates that the skin friction coefficient at the wavy wall exhibits a smooth nonlinear dependence on the governing parameters. The heat source parameter (Q) and Prandtl number (Pr**)** both reduce the skin friction coefficient, while the Grashof number **(**Gr**)** slightly enhances the wall shear stress through buoyancy effects. Among the investigated interactions, the Q-Pr combination exhibits the most noticeable nonlinear behaviour, whereas the interactions involving Gr are comparatively weak, as evidenced by the nearly parallel contour lines. The absence of abrupt peaks or valleys demonstrates stable behaviour across the design space and confirms that the quadratic response surface model provides an adequate representation of the wall skin friction characteristics.

The response surface plots in Figures 28-33 represent the skin friction coefficient at (y = 1) as a function of Reynolds number (Re), Grashof number (Gr), Heat source parameter (Q), and Prandtl number (Pr).

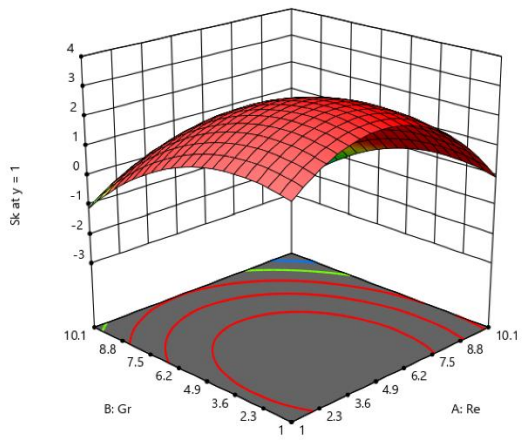

Fig. 28 Skin friction at y = 1 for various Re

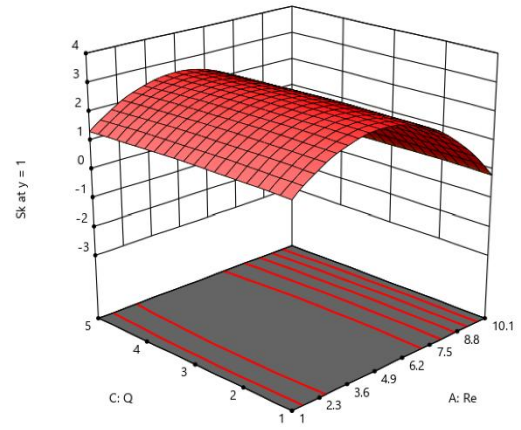

Fig. 29 Skin friction at y = 1 for various Q

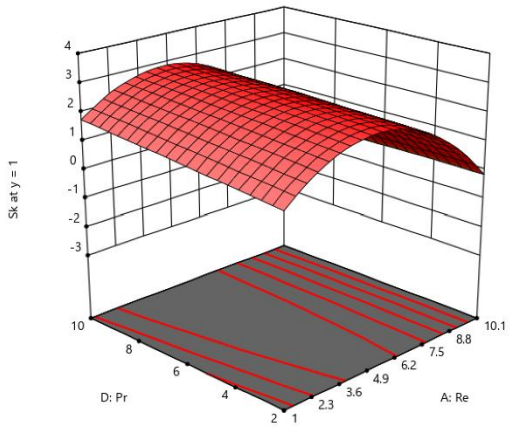

Fig. 30 Skin friction at y = 1 for various Pr

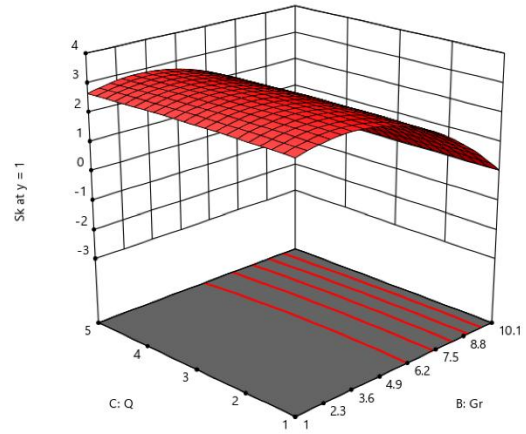

Fig. 31 Skin friction at y = 1 for various Q

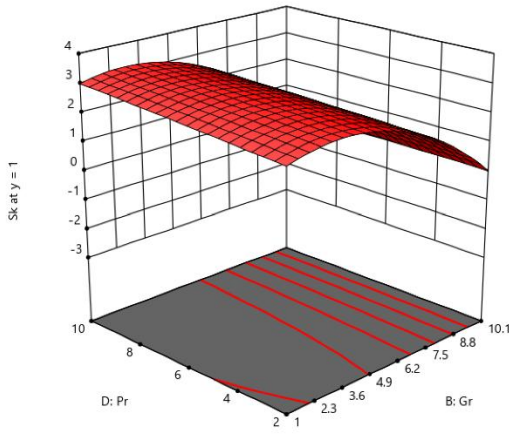

Fig. 32 Skin friction at y = 1 for various Gr

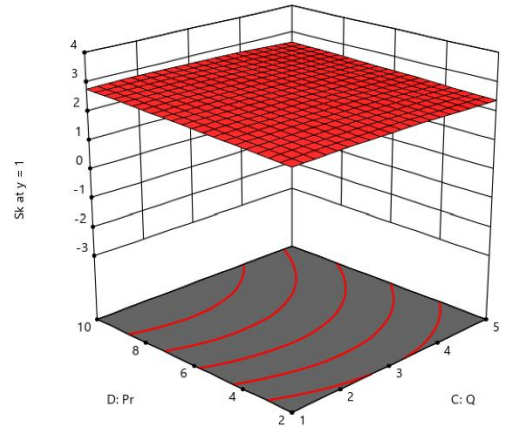

Fig. 33 Skin friction at y = 1 for various Pr

The response surface analysis shows that the Reynolds number is the dominant factor controlling the skin friction coefficient at (y=1). The response exhibits a pronounced quadratic dependence on Reynolds number, with maximum skin friction occurring at intermediate Reynolds numbers. The Grashof number generally causes a slight reduction in skin friction, whereas the Prandtl number produces a small positive influence. The heat source

parameter has only a minor effect throughout the investigated range. Most contour plots consist of nearly parallel lines, indicating weak interaction effects among the variables, while the dome-shaped surfaces involving Reynolds number confirm the significance of its quadratic contribution. Overall, the fitted quadratic response surface adequately represents the nonlinear variation of the skin friction coefficient at y = 1.

7. Conclusion

The investigated design space's complex, nonlinear fluid flow and heat transfer characteristics were accurately captured and predicted using the quadratic Response Surface Methodology (RSM). The smooth curvatures and stable response profiles across all analysed parameters validate the adequacy and reliability of the quadratic model.

The primary findings from the response surface analysis are as follows:

- The transverse coordinate (y) exerts the most dominant influence on fluid velocity, followed closely by the Reynolds number (Re), Heat source parameter (Q) shows a moderate impact, while the Grashof number (Gr) has the least influence.
- Similar to velocity, the transverse coordinate (y) has the most significant positive impact on temperature. Reynolds number exhibits a moderate inverse effect due to enhanced convective cooling, while Gr and Q play minor roles.
- At the wavy Plate, Re and Pr are the dominant factors. Re exhibits an optimal threshold beyond which heat transfer decreases, while increasing Pr consistently enhances Nu by reducing thermal boundary layer thickness.
- At the wall (y=1), Re has the most of a negative effect, while Pr has the most of a positive effect. Gr and Q have effects that range from mild to moderate, and overall, they have interactions that range from weak to moderate.
- At the wavy wall, both Q and Pr reduce skin friction, while Gr slightly enhances it via buoyancy effects. The Pr interaction demonstrates the most prominent nonlinear behaviour.
- At the wall (y=1), Re is the absolute dominant factor, displaying a dome-shaped quadratic dependence where maximum skin friction occurs at intermediate Reynolds numbers. In contrast, Gr has a small positive effect on skin friction, Pr has a small positive effect, and Q has no effect at all.

Overall, the study demonstrates that fluid flow, heat transfer rate, and wall shear stresses are highly sensitive to nonlinear variations in governing parameters, with the quadratic RSM model serving as a robust tool for predicting these transport phenomena without unexpected abrupt transitions.

REFERENCES

1. Asako, Y., & Faghri, M. (1987). Three-dimensional heat transfer and fluid flow analysis of arrays of rectangular blocks encountered in electronic equipment. International Journal of Heat and Mass Transfer, 30(11), 2429–2439. https://doi.org/10.1016/0017-9310(87)90231-1
2. Attia, H. A. (2006). Unsteady MHD flow and heat transfer of a dusty fluid between parallel plates with variable physical properties. Communications in Nonlinear Science and Numerical Simulation, 11(1), 102–118. https://doi.org/10.1016/j.cnsns.2004.06.002
3. Benjamin, T. B. (1959). Shearing flow over a wavy boundary. Journal of Fluid Mechanics, 6(2), 161–205. https://doi.org/10.1017/S002211205900057X
4. Borkakati, A. K., & Pop, I. (1984). Unsteady hydromagnetic flow of a dusty viscous fluid past an infinite wavy wall. Acta Mechanica, 51(3-4), 163–173. https://doi.org/10.1007/BF01174648
5. Burns, S. P., & Dutcher, C. R. (2010). Geometric optimization of laminar flow profiles inside periodic wavy-walled channels. Journal of Fluids Engineering, 132(12), 121202.https://doi.org/10.1115/1.4003063
6. Chamkha, A. J. (2000). Flow of a two-phase gas-particle mixture in a porous-walled channel. Journal of Fluids Engineering, 122(2), 312–319. https://doi.org/10.1115/1.483259
7. Datta, N., & Mishra, S. K. (1982). Boundary layer flow of a dusty fluid over an oscillating flat plate. Acta Mechanica, 42(1-2), 71–83. https://doi.org/10.1007/BF01170470
8. Ghosh, A. K., & Debnath, L. (2004). Unsteady hydromagnetic flow of a dusty fluid between two oscillating plates in a rotating system. Applied Mathematics and Computation, 154(3), 749–767. https://doi.org/10.1016/S0096-3003(03)00748-4
9. Gireesha, B. J., Chamkha, A. J., & Manjunatha, S. (2012). Effect of radiation on MHD flow and heat transfer of a dusty fluid over a stretching sheet. International Journal of Numerical Methods for Heat & Fluid Flow, 22(4), 491–506 https://doi.org/10.1108/09615531211218151

10. Hayat, T., Iqbal, Z., & Mustafa, M. (2012). Flow of a dusty fluid over a stretching sheet with thermal radiation. Journal of Aerospace Engineering, 25(3), 416–422. https://doi.org/10.1061/(ASCE)AS.1943-5525.0000140
11. Healy, J. V., & Yang, H. T. (1970). Oscillatory motion of a dusty gas. Astronautica Acta, 15(4), 315–325. https://scholar.google.com/scholar?q=%22Oscillatory+motion+of+a+dusty+gas%22+Healy+Yang+1970&utm_source=chatgpt.com
12. Mahanthesh, B., Gireesha, B. J., & Gorla, R. S. R. (2017). Non-linear radiative heat transfer in MHD three-dimensional flow of a dusty nanofluid over a stretching sheet. Journal of the Nigerian Mathematical Society, 36(1), 101–121. https://doi.org/10.1016/j.jnnms.2016.02.003
13. Michael, D. H. (1965). Kelvin-Helmholtz instability of a dusty gas. Proceedings of the Cambridge Philosophical Society, 61(2), 569–571. https://doi.org/10.1017/S030500410000416X
14. Nield, D. A., & Kuznetsov, A. V. (2009). Thermal non-equilibrium in porous media: An overview. International Journal of Heat and Mass Transfer, 52(21-22), 5080–5085. https://doi.org/10.1016/j.ijheatmasstransfer.2009.04.027
15. Nishimura, T., Ohori, Y., & Kawamura, Y. (1984). Flow characteristics in a channel with symmetric sinusoidal wavy walls for steady flow. Journal of Chemical Engineering of Japan, 17(5), 466–471. https://doi.org/10.1252/jcej.17.466
16. Ramesh, G. K., Gireesha, B. J., & Bagewadi, C. S. (2012). Heat transfer in a dusty fluid flow over a stretching sheet with non-uniform heat source/sink. International Journal of Multi-Phase Flow, 40(1), 112–120. https://doi.org/10.1016/j.ijmultiphaseflow.2011.11.008
17. Rashidi, M. M., Freidoonimehr, N., Hosseini, A., Anwar Bég, O., & Gorla, R. S. R. (2014). Analysis of entropy generation in MHD blood flow through a porous segmented channel. Journal of Mechanics in Medicine and Biology, 14(06), 1450085. https://doi.org/10.1142/S021951941450085X
18. Saffman, P. G. (1962). On the stability of laminar flow of a dusty gas. Journal of Fluid Mechanics, 13(1), 120–128. https://doi.org/10.1017/S002211206200008X
19. Siddiqa, S., Hossain, M. A., & Saha, S. C. (2015). Two-phase natural convection flow of a dusty non-Newtonian fluid along a vertical surface. International Journal of Heat and Mass Transfer, 89(1), 1104–1111. https://doi.org/10.1016/j.ijheatmasstransfer.2015.06.012
20. Turkyilmazoglu, M. (2012). Exact analytical solutions for heat and mass transfer of dusty fluid flow over a stretching surface. Chemical Engineering Science, 71(1), 221–229. https://doi.org/10.1016/j.ces.2011.12.029
21. Umavathi, J. C., Kumar, J. V., & Pop, I. (2005). Mixed convection in a vertical channel filled with a porous medium bounded by a wavy wall. International Journal of Heat and Mass Transfer, 48(7), 1402–1412. https://doi.org/10.1016/j.ijheatmasstransfer.2004.09.043
22. Vajravelu, K., & Sastry, K. S. (1978). Free convective heat transfer to a steady laminar flow of a viscous fluid heat-generating fluid in a vertical channel bounded by a wavy wall and a flat wall. International Journal of Heat and Mass Transfer, 21(5), 611–618. https://doi.org/10.1016/0017-9310(78)90057-0
23. Wang, C. C., & Chen, C. K. (2002). Forced convection in a wavy-walled channel. International Journal of Heat and Mass Transfer, 45(12), 2587–2595. https://doi.org/10.1016/S0017-9310(01)00334-0

Appendix

$$m_1 = \sqrt{QPrRe}$$

$$m_2 = -\sqrt{QPrRe}$$

$$B_1 = e^{m_2} - e^{m_1}$$

$$A_1 = {-1}/{B_1}$$

$$A_2 = -A_1$$

$$A_4 = \frac{Gr}{Re}\frac{A_1}{{m_1}^2}(e^{m_1} - e^{m_2})$$

$$B_2 = A_1 m_1 + A_2 m_2$$

$$A_5 = {B_2\, e^{m_2}}/{B_1}$$

$$A_6 = {-B_2\, e^{m_1}}/{B_1}$$

$$B_3 = \frac{Gr}{Re}\left(\frac{A_5}{{m_1}^2} + \frac{A_6}{{m_2}^2}\right) - \left(A_4 - \frac{Gr}{Re}\frac{A_1}{{m_1}^2}(m_1 - m_2)\right)$$

$$A_7 = B_3$$

$$B_4 = -A_{7+}\frac{Gr}{Re}\left(\frac{A_5}{{m_1}^2}e^{m_1} - \frac{A_6}{{m_2}^2}e^{m_2}\right)$$

$$A_8 = B_4$$